

# Monte Carlo study of the effect of an applied field on the molecular organization of polymer-dispersed liquid-crystal droplets

E. Berggren and C. Zannoni

*Dipartimento di Chimica Fisica ed Inorganica, Università di Bologna, Viale Risorgimento 4, 40136 Bologna, Italy*

C. Chiccoli, P. Pasini, and F. Semeria

*Istituto Nazionale di Fisica Nucleare, Sezione di Bologna, Via Irnerio 46, 40126 Bologna, Italy*

(Received 7 June 1993)

We have studied the effect of an applied field on a system of particles interacting with a Lebwohl-Lasher potential, enclosed in a polymer-dispersed liquid-crystal droplet with radial boundary conditions. We have used Monte Carlo simulations on a wide temperature range for systems of  $N = 304$  and 5832 particles with positive susceptibility anisotropy, and we have calculated order parameters, the molecular organization, and powder-type deuterium NMR line shapes for eight different field-strength values. The effect of the field on the molecular organization is discussed.

PACS number(s): 61.30.Gd, 61.30.Jf, 64.70.Md

## I. INTRODUCTION

Polymer-dispersed liquid crystal droplets (PDLC) consist of submicrometer or micrometer size droplets of low-molecular-weight liquid crystals embedded in a polymer matrix [1]. They are attracting considerable attention in view of their applications in display technology and in other optical devices such as, for example, switchable windows [1–7]. From a fundamental point of view they offer a stimulating field of investigation concerning the behavior of mesophases in a restricted environment [8–10]. Various kinds of boundary condition at the liquid-crystal-polymer interface have been realized with a suitable choice of the polymer and of the preparation method. The more common boundary conditions, each one with a different influence on the molecular organization inside the droplets, are the following: (i) *radial*, with the molecules at the polymer interface oriented normal to the local surface, thus pointing toward the center of the droplet; (ii) *toroidal*, where the particles at the interface lie in planes perpendicular to the  $z$  axis while having orientations tangential to the droplet surface; and (iii) *bipolar*, where the molecules at the surface are again tangent to the sphere but are directed along the meridians towards the poles.

The surface boundary conditions will tend to influence the orientation of molecules near the surface and the aligning effect may propagate inside the droplet. In general there will be a competition between the molecular orientation induced by the surface boundary conditions, the effects of ordering of the liquid crystal itself due to the molecules trying to arrange parallel to each other, and the disordering effect of temperature. The resulting molecular organization for a certain boundary condition will depend on a number of factors, including the strength of the surface interaction, the temperature, and so on. Thus it is not easy to predict the actual molecular organization with available theories and even, especially for the smaller sizes, to investigate it experimentally [6,7].

We have shown in a series of recent papers [11–14] that Monte Carlo (MC) simulations can be a particularly effective tool to predict the combined effect of these factors without resorting to continuum theory, whose applicability on such small scales is not obvious. In particular we have investigated, using Monte Carlo simulations, the molecular organization in droplets with radial [11,12] and tangential [13] boundary conditions.

The changes in texture and molecular organization produced by the application of an external field have been the subject of various theoretical [14,15] and experimental studies [7,16–20]. In particular Dubois-Violette and Parodi have predicted that a nematic droplet with radial boundary conditions and positive susceptibility anisotropy will undergo a first order transition to an axial structure as the field strength increases [15]. In a preliminary work [14] we have also started to investigate the effects of the application of an external field to the droplets. Here we present a detailed investigation of the molecular organization and the calculation of the thermodynamic observables for this last case.

The paper is organized as follows: In Sec. II we describe the model used in our work; in Sec. III the details of the simulations are presented, while Secs. IV and V are devoted to a description of the results. Finally a discussion and conclusion are presented in Sec. VI.

## II. MODEL

We consider a lattice model of PDLC, where the particles are treated as interaction sites (“spins”) with continuously varying orientation but with positions fixed, because we intend to concentrate on orientational phenomena and because, as we know from a number of simulations used to study liquid crystals [11–14], this kind of model has several features that are important in our case. The first and most important one is that these models can successfully reproduce the nematic-isotropic transition and the orientational order as a function of

temperature. Moreover a large number of particles can be treated, while using more realistic potentials only much more limited samples can be simulated. Another advantage associated with the reduced computational burden arises when, as in the present case, simulations over a large temperature range are required for a number of external conditions, here field strengths.

In our studies the particles, placed at the sites of a cubic lattice and taken to be cylindrically symmetric, interact through the following attractive nearest-neighbor Lebwohl-Lasher (LL) pair potential [21]:

$$U_N = - \sum_{\substack{i,j \\ i < j}} \epsilon_{ij} P_2(\cos \beta_{ij}), \quad (2.1)$$

where  $\epsilon_{ij}$  is a positive constant  $\epsilon$  for nearest-neighbors particles  $i$  and  $j$  and zero otherwise,  $\beta_{ij}$  is the angle between the axis of the two spins, and  $P_2$  is a second-rank Legendre polynomial. It is a well studied model that represents the prototype for the nematic isotropic orientational phase transition. In the bulk it reproduces the weak first order transition, observed for real nematics, at a reduced temperature  $T^* = 1.1232$  [22]. The LL model and its transition properties have recently attracted a renewed interest from various groups [23,24].

In order to simulate model droplets we take a jagged sphere obtained from a cubic lattice by considering all the molecules falling within a given range from the chosen center.

The different boundary conditions are imposed in general by assuming a layer of outside particles with a fixed orientation determined by the specific type of surface assumed. In the present case radial boundaries have been simulated by having these outside molecules pointing toward the center.

We have chosen to mimic the effect of an external electric or magnetic field by summing an additional second-rank term to the model Hamiltonian:

$$U_N = - \sum_{\substack{i,j \\ i < j}} \epsilon_{ij} P_2(\cos \beta_{ij}) - \epsilon \xi \sum_{i=1}^N P_2(\cos \beta_i), \quad (2.2)$$

Here  $\beta_i$  is the angle between the field direction and the molecular symmetry axis and  $\xi$  determines the strength of coupling with the field  $\mathbf{B}$ , which is assumed to be homogeneous across the drop. The parameter  $\xi$  would depend in a real situation on the anisotropy of the electric or magnetic susceptibility and on the field intensity. For a magnetic field

$$\epsilon \xi = \frac{1}{3} \frac{\Delta \kappa}{\mu_0} \mathbf{B}^2, \quad (2.3)$$

where  $\mathbf{B}$  is the magnetic induction and  $\Delta \kappa$  is the molecular magnetic polarizability anisotropy [25] and it is assumed that the macroscopic diamagnetic anisotropy  $\Delta \chi$  is the average of independent molecular contributions.

For alignment in an electric field the interaction of the system with the field is described macroscopically by the dielectric anisotropy  $\Delta \epsilon$  at that frequency. The microscopic interpretation is complicated in general by internal

field and nonadditivity problems, especially in the case of polar molecules and writing the molecular level equivalent of the interaction as a sum of independent terms is not necessarily allowed. On the other hand, in the case of nonpolar compounds the field contribution to the total energy of the system can to a good approximation be written as in Eq. (2.1), since the dielectric constant is essentially determined by a sum of the microscopic polarizability anisotropy  $\Delta \alpha$  contributions [25]. In that case an identification of the field term in Eq. (2.1) with molecular quantities would give

$$\epsilon \xi = \frac{\epsilon_0}{3} \Delta \alpha \mathbf{E}^2. \quad (2.4)$$

In practice it will be somewhat easier to use electric rather than magnetic fields. The effect of an electric field of  $1 \text{ V}/\mu\text{m}$  has been found to be equivalent to that of a 10-T magnetic field for the liquid-crystal mixture E7 [7] in the sense that at macroscopic level

$$\epsilon_0 \Delta \epsilon \mathbf{E}^2 = \frac{\Delta \chi}{\mu_0} \mathbf{B}^2, \quad (2.5)$$

where  $\Delta \epsilon$  is the dielectric constant anisotropy. Here we consider a positive coupling term  $\xi$  so that the field has the effect of favoring alignment of the particles parallel to its direction.

This Hamiltonian has been used some years ago to investigate the field effect on bulk nematic by Monte Carlo [26,27] and to study, using mean field theory, very different effects such as laser self-focusing in liquid crystals [28] and the effect of the cholesterol in lipid membranes [29]. Thus we hope that our results can be indirectly useful in these other fields as well.

### III. SIMULATIONS

We have performed a complete set of Monte Carlo simulations for eight different values of  $\xi$  (0, 0.01, 0.05, 0.1, 0.15, 0.2, 0.3, 0.5) and for two different sample sizes:  $N = 304$  and  $N = 5832$  (15 temperatures have been studied for the large and 60 for the small sample). A number of other cases have been studied for lower field strength ( $\xi = 0.001, 0.005, 0.02, 0.03, 0.04$ ) and  $N = 5832$  particles at selected temperatures. Several runs ( $\xi = 0.01, 0.05, 0.1, 0.2, 0.4$ ) have been performed with  $N = 1476$  to look at droplet size effects.

The simulations for different couplings are completely independent from each other. The calculation starts from a perfect hedgehog system at low temperatures or, when available, from an already equilibrated configuration at the nearest lower temperature. The Metropolis procedure [30] is then used to update the lattice for a certain number of cycles, i.e., of sets of  $N$  attempted moves. Each particle is selected at random for a trial move at every cycle using a random shuffling algorithm [31]. A new trial orientation of the chosen particle is then generated by a controlled variation from the previous one using the Barker-Watts technique [32]. We have checked that a rejection ratio not too far from 0.5 is achieved with a feedback algorithm implemented.

As usual a number of simulation runs are performed to reach equilibrium, where the thermodynamic observables fluctuate around their mean values. For the smaller systems we have discarded about 15 000 cycles at each temperature, while 10 000 cycles have been employed to produce the average observable results. For the larger size systems ( $N = 5832$ ) we have discarded at least 30 000 equilibrium cycles before starting production runs of about 15 000 cycles. During the production run various observables have been calculated in addition to the internal energy, needed for the Monte Carlo procedure. The property of interest  $A$  is evaluated at every cycle. After a certain number of cycles (typically between 100 and 2000) an average  $A^J$  is calculated thus providing an effective coarse graining of the trajectory. A further grand average is then computed as the weighted average over  $M$  such supposedly uncorrelated segments. The attendant weighted standard deviation from the average  $\sigma_A$  is also calculated and gives the error estimates shown in the figures.

#### IV. RESULTS

A number of properties are calculated, as we shall see in detail later on; in general they can be divided in single-particle and multiparticle (typically configurations or two-particle observables) ones. More specifically, one-particle tensor properties of second- and fourth-rank are calculated.

##### A. Heat capacity

The energy of the system is calculated from Eq. (2.2). The results are not reported for reason of space, but are used to obtain the dimensionless specific heat  $C_V^*$ , shown in Fig. 1, by differentiating the average energy with respect to temperature. As observed in our previous papers on nematic droplets [11,12], the heat capacity results

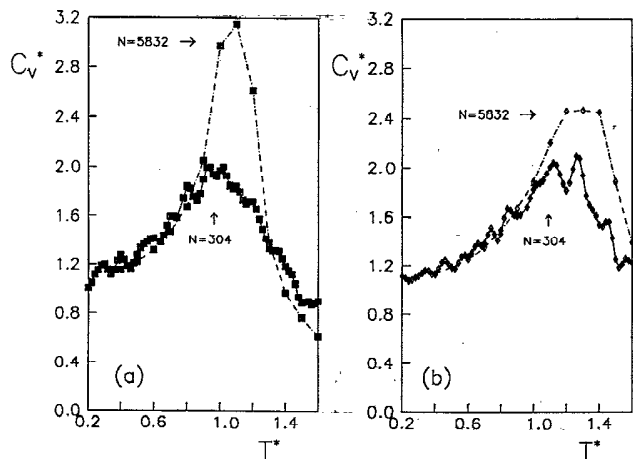


FIG. 1. The temperature dependence of the specific heat  $C_V^*$  for two selected field strengths (a)  $\xi = 0.01$  and (b)  $\xi = 0.50$  for two system sizes  $N = 304$  and  $N = 5832$ .

do not present a marked dependence on the lattice size: the shape of the curves is quite symmetric with a clear indication of the absence of a phase transition. By comparison we recall that MC data for the bulk Lebwohl-Lasher model show a strong size dependence [33]. In that case the  $C_V^*$  curve is not symmetric with a well pronounced peak that rapidly grows and sharpens as the number of particles increases. For a sample with more than 5000 particles the bulk (i.e., periodic [22] or Cluster Monte Carlo [33]) boundary conditions give a heat capacity maximum well above 20 in dimensionless units. The smoothening of the transition is thus due not only to size effects, but also to surface conditions [34–36]. In Figs. 1(a) and 1(b) the results for the two system sizes and for two values of the field strength are reported.

We can observe that the main effect of the external field is a shifting of the maximum of the curve toward higher temperatures [see Figs. 2(a) and (b)] as we could expect from a stabilization of the ordered phase upon increasing the strength of the field. The behavior is different for the two sample sizes, with a more discontinuous character for the larger one. An increase of the field also causes a further smoothening out of the pseudotransition that becomes continuous as the supposed isotropic phase is itself ordered by the field. This indication is confirmed by the observation that the  $C_V^*$  maximum is slightly lower for the higher field strengths examined.

##### B. Order parameters

We calculate second- and fourth-rank orientational order parameters  $\langle P_2 \rangle_\lambda$  and  $\langle P_4 \rangle_\lambda$ , obtained from a diagonalization of the ordering matrix as described in detail in Ref. [22]. This gives an indication of the order with respect to the instantaneous director and it does not have an immediate significance [11] for droplets with radial boundary conditions and in the absence of an external field when, especially at the low temperatures, the effect

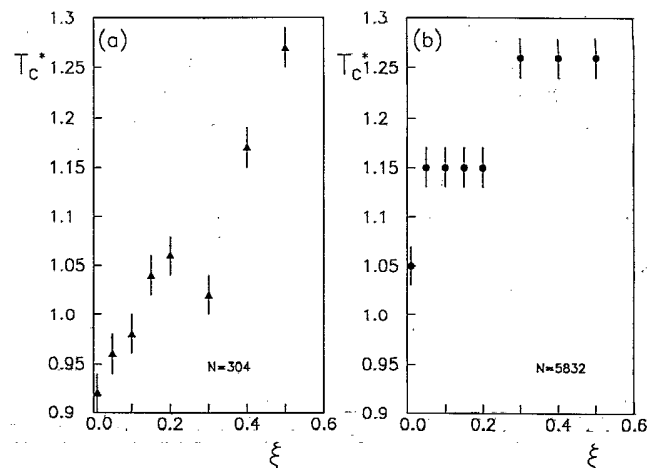


FIG. 2. The field-strength dependence of the temperature at which the maximum of the heat capacity occurs, reported for the two system sizes studied [plates (a) and plate (b)].

of the ordering of the molecules at the interface dominates.

Increasing the field strength the molecules tend to align with respect to the field direction which then becomes coincident with the director. Thus we also consider another order parameter:  $\langle P_2 \rangle_B$ , expressing the molecular alignment with respect to the field direction [14]:

$$\langle P_2 \rangle_B = \frac{1}{N} \sum_{i=1}^N P_2(\mathbf{u}_i \cdot \hat{\mathbf{B}}), \quad (4.1)$$

where  $\mathbf{u}_i$  is the orientation vector of the  $i$ th particle axis and  $\hat{\mathbf{B}}$  is a unit vector along the field direction [in the present study we have chosen the field along the  $z$  axis so  $\mathbf{B} = (0, 0, 1)$ ]. We expect  $\langle P_2 \rangle_B$  to be vanishingly small when the field applied is very low, while it should become closer and closer to the value of the usual order parameter  $\langle P_2 \rangle_\lambda$  as the field increases.

To express disordering from the perfect hedgehog organization, correspondent to the configuration expected at low temperature and in absence of an external field, we have calculated a *radial order parameter*  $\langle P_2 \rangle_R$  [11] defined as follows:

$$\langle P_2 \rangle_R = \frac{1}{N} \sum_{i=1}^N P_2(\mathbf{u}_i \cdot \mathbf{r}_i), \quad (4.2)$$

where  $N$  is the number of particles contained in the sphere and  $\mathbf{r}_i$  is the radial vector of the  $i$ th particle. It is a quantitative indication of the radial ordering, which has a maximum when all the particles are along their radial vector and its temperature dependence has a typical order parameter behavior.

Increasing the field strength, also at low temperature, the molecular organization is more influenced by the second term in Eq. (2.2).

The results for the order parameters  $\langle P_2 \rangle_B$  and  $\langle P_2 \rangle_R$  are shown in Fig. 3 for the eight values of  $\xi$  for which we have performed a complete simulation. We do not present the plot of  $\langle P_2 \rangle_\lambda$  because, except for the lowest values of  $\xi$ , it is essentially undistinguishable from that of  $\langle P_2 \rangle_B$ .

The radial order parameter  $\langle P_2 \rangle_R$  [Fig. 3(a)] shows a standard behavior for low  $\xi$ : it starts from a value close to one at very low temperatures and goes to its minimum at temperatures correspondent to the isotropic phase. Increasing the field this behavior becomes progressively less evident up to the highest field strength considered ( $\xi = 0.5$ ) for which the curve is essentially flat. All the curves join in the isotropic phase where the value of the order parameter is limited from the number of particles.

The order parameter with respect to the field direction  $\langle P_2 \rangle_B$  [Fig. 3(b)] shows the opposite behavior. It is not well defined for low  $\xi$  and assumes, of course, a more usual trend for high  $\xi$ . The  $\langle P_2 \rangle_B$  curves are well separated also in the (pseudo)isotropic phase because the field induces an additional ordering also in this region of temperatures, that is, in turn manifested in  $\langle P_2 \rangle_B$ . The curve for  $\xi = 0.01$  is apparently anomalous, with an initial increase of the order parameter as the temperature

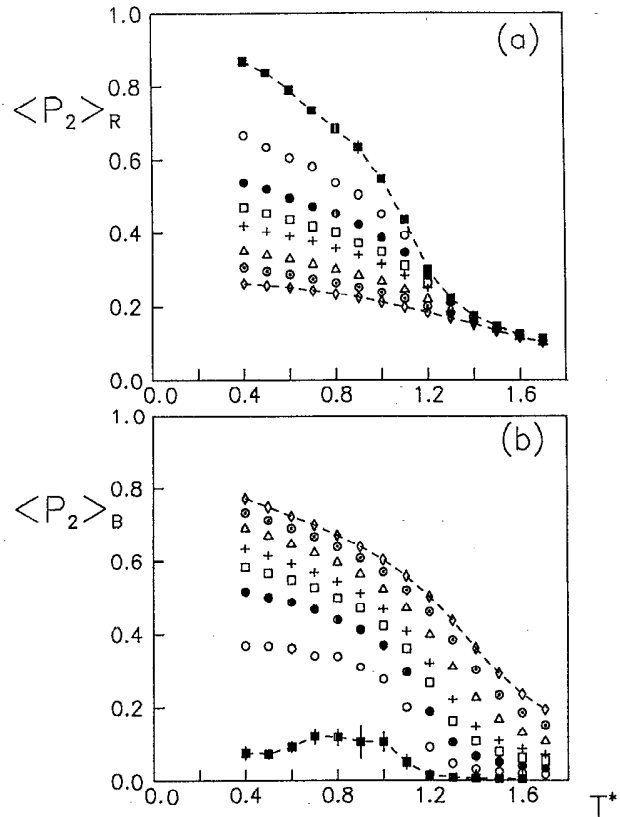


FIG. 3. The (a) radial  $\langle P_2 \rangle_R$  and (b) field  $\langle P_2 \rangle_B$  order parameter for various external field strengths  $\xi$  as a function of reduced temperature  $T^* = kT/\epsilon$ . The different values of field strengths are  $\xi = 0.001$  ( $\blacksquare$ ),  $\xi = 0.05$  ( $\circ$ ),  $\xi = 0.10$  ( $\bullet$ ),  $\xi = 0.15$  ( $\square$ ),  $\xi = 0.20$  ( $+$ ),  $\xi = 0.30$  ( $\triangle$ ),  $\xi = 0.40$  ( $\odot$ ), and  $\xi = 0.50$  ( $\diamond$ ).

increases. However, at this low strength  $\langle P_2 \rangle_B$  is not very meaningful, since the system is essentially unaffected by the field.

To look at the field dependence of the order parameter  $\langle P_2 \rangle_B$  we have analyzed the results at two selected temperatures, one below ( $T^* = 0.4$ ) and one above ( $T^* = 1.4$ ) the heat capacity maximum. We report these results, for three different system sizes, in Fig. 4 and we can observe, at the lower temperature [Fig. 4(a)], a saturation with the field strength while at  $T^* = 1.4$  [Fig. 4(b)] order increases linearly with the field.

It is also clear that the size effects are important here and that the radial boundary condition has a stronger influence on the ordering as the system is smaller.

Of particular interest is how the order parameters change across the droplet. We have investigated the variation of the order parameters from the center of the droplet to the surface. To do that we have divided the sample in a set of concentric shells in an onion skin fashion [13]. More specifically, we have defined four spherical shells for the smaller system and twelve shells for the larger one. Then the orientational order parameters  $\langle P_2 \rangle_\lambda$ ,  $\langle P_2 \rangle_R$ , and  $\langle P_2 \rangle_B$  have been calculated for these different regions and are shown in Fig. 5 for the  $N = 5832$  droplet at various field strengths and at temperature  $T^* = 0.4$ .

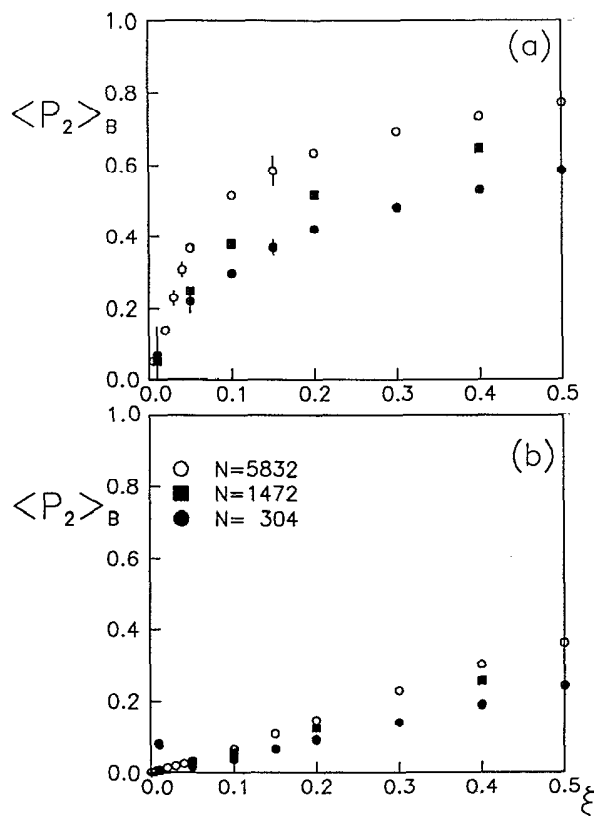


FIG. 4. The second-rank field order parameter  $\langle P_2 \rangle_B$  obtained from MC simulations of three different lattice sizes  $N$  vs the field strength  $\xi$ . The results at (a) low temperature  $T^* = 0.4$  and (b) temperature above the heat capacity anomaly  $T^* = 1.4$  are reported.

$\langle P_2 \rangle_R$  is very small near the center, showing that little radial order exists at low values of field strength. As  $r$  is increased and the radially ordered boundary is approached  $\langle P_2 \rangle_R$  increases and saturates as predicted by Schopol and Sluckin [8]. This behavior is compatible with a central ordered core in the direction of the field as indicated by  $\langle P_2 \rangle_B$  in Fig. 5(b). The size of the ordered core increases as the field strength increases up to the highest value of  $\xi$  considered for which the majority of the particles inside the droplet are aligned with the field direction. In this case  $\langle P_2 \rangle_R$  increases only as the shell on which it is calculated approaches the surface. Once again the field order parameter  $\langle P_2 \rangle_B$  shows the opposite behavior.

### C. Orientational pair correlations

Another useful way of looking at changes in molecular organization across the droplet is through the two particle angular correlations coefficients  $G_L(r)$ . In general these describe a set of expansion coefficients of the rotationally invariant pair correlation function [27],

$$G(r, \omega_{12}) = \frac{G_0^{00}(r)}{\int d\omega_1 d\omega_2} \sum_L (2L+1) G_L(r) P_L(\cos \beta_{12}), \quad (4.3)$$

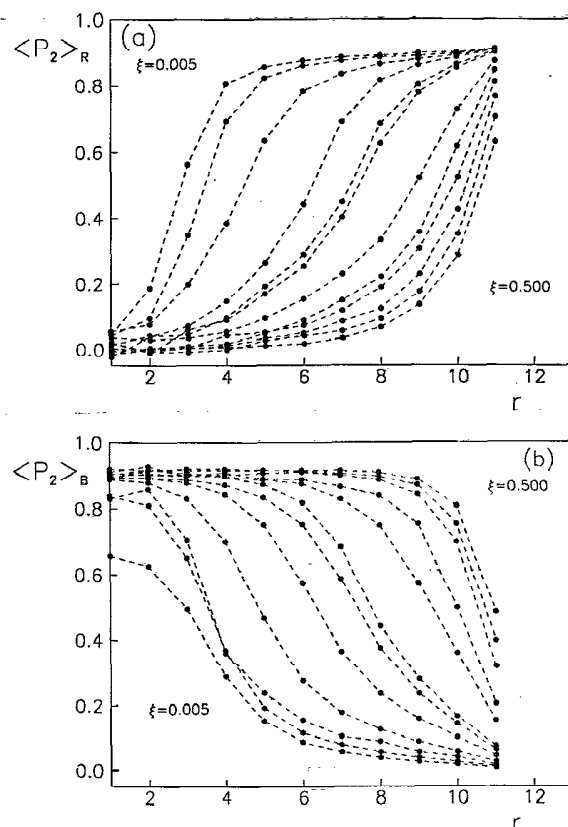


FIG. 5. Order parameters (a)  $\langle P_2 \rangle_R$  and (b)  $\langle P_2 \rangle_B$  against distance from the center  $r$  (in lattice units) for a RBC droplet with  $N = 5832$  particles and for different field strengths at reduced temperature  $T^* = kT/\epsilon = 0.4$ . In (a) the values of  $\xi$  from top to bottom are 0.005, 0.010, 0.020, 0.030, 0.040, 0.050, 0.100, 0.150, 0.200, 0.300, 0.400, and 0.500. In (b) the values of  $\xi$  are the same, but in reversed order.

where  $\omega_i$  is the set of Euler angles needed to specify the orientation of molecule  $i$  and  $\omega_{12}$  is the relative orientation of the two particles at distance  $r$ . The coefficients  $G_L(r)$  are two-particle order parameters

$$G_L(r) = \frac{1}{G_0^{00}(r)} \int d\omega_1 d\omega_2 G(r, \omega_{12}) P_L(\cos \beta_{12}) \quad (4.4)$$

and  $G_0^{00}(r)$  is the radial distribution, which for a lattice simply counts the number of neighbors in progressively larger shells [22]. In a uniform system the various  $G_L(r)$  give the correlation between the relative orientation  $\beta_{12}$  of two arbitrary particles separated by a distance  $r$ . Here we wish to investigate the correlations between the orientation of particles at a distance  $r$  from the center with those at the center itself. In practice for the calculation of pair correlations,  $M = 8$  particles nearest the droplet center are selected as origins and the pair correlations with all the other particles within a certain range are calculated.

More in detail we use the following algorithm.

(i) Choose the  $M$  particles closest the drop center as origins.

(ii) Now choose an origin on particle  $i$  and consider spherical layers of a certain resolution  $\Delta r$ .

(iii) Count the number of particles  $n_{r_i}$  within the layer (this is done beforehand).

(iv) Calculate for each particle  $j$  falling within the layer the Legendre polynomial  $P_L(\cos \beta_{ij})$  with respect to the origin particle  $i$  and accumulate its contribution to the average.

(v) Repeat for all the particles in the sample.

(vi) Repeat for all origins and obtain the total average. Thus

$$G_L(r) = \langle P_L(\cos \beta_{12}) \rangle_r \quad (4.5a)$$

$$= \frac{1}{M} \sum_{i=1}^M \frac{1}{n_{r_i}} \sum_{j (\neq i)}^N P_L(\cos \beta_{ij}) \Delta(r_{ij} - r) \quad (4.5b)$$

with rank  $L = 2$  and 4. The fuzzy delta function  $\Delta(r_{ij} - r)$  is defined to be 1 when  $r_{ij}$  belongs to the layer centered at  $r$  and zero otherwise. As we can guess from the above formulas, the calculation is quite time consuming and represents a relevant percentage of the total time spent in the simulation.

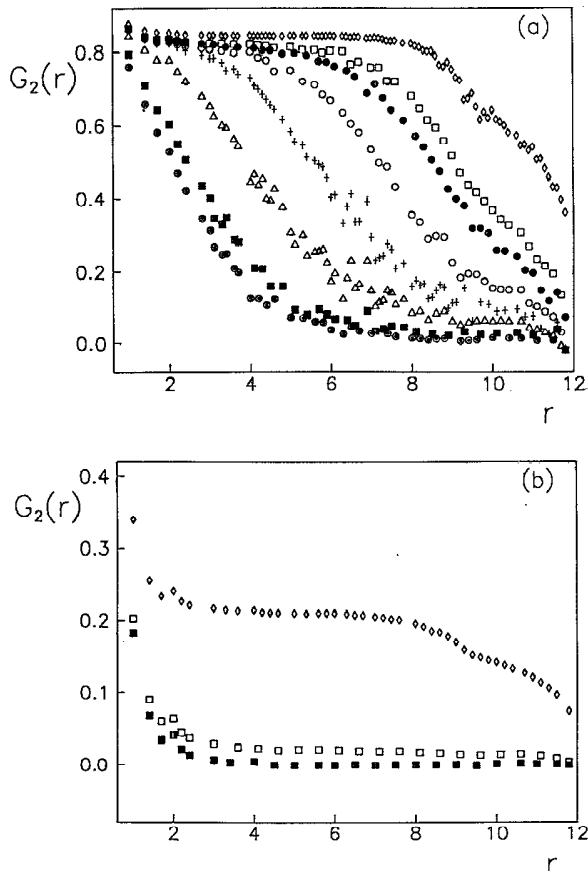


FIG. 6. The second-rank pair correlation coefficient  $G_2(r)$  between a particle at the center and one at separation  $r$  in lattice units as obtained from the MC simulation with  $N = 5832$  particles at  $T^* = 0.40$  (a) and 1.40 (b). The results for various field strengths,  $\xi = 0.00$  ( $\odot$ ),  $\xi = 0.01$  ( $\blacksquare$ ),  $\xi = 0.02$  ( $\triangle$ ),  $\xi = 0.03$  ( $+$ ),  $\xi = 0.05$  ( $\circ$ ),  $\xi = 0.10$  ( $\bullet$ ),  $\xi = 0.15$  ( $\square$ ), and  $\xi = 0.5$  ( $\diamond$ ), are shown. In plate (b) all curves in the range  $0.01$  ( $\blacksquare$ )  $< \xi < 0.15$  ( $\square$ ) are not shown for clarity.

Here we have calculated the first two angular pair correlation coefficients  $G_2(r)$  and  $G_4(r)$  for all the temperatures, even if only  $G_2(r)$  is shown for reasons of space. The overall results for  $G_2(r)$  are presented in Fig. 6 for two selected temperatures. In a uniform system with periodic boundary conditions the pair coefficients  $G_L(r)$  start from one and tail off to essentially  $\langle P_L \rangle^2$  in the nematic phase [23]. Here the particles at the boundary point towards the center so the particle chosen as the origin will not be correlated with those at that distance. Given that  $G_2$  starts from one we would expect a rapid decay of  $G_2$  in the absence of an ordered domain in middle and viceversa.

Looking at our results we see that the effect of the external field on the correlation functions is greater at low temperature [see Fig. 6(a)] where there is an effective competition with the boundary conditions that try to produce a radial ordering inside the droplet. Thus for very low field strengths the molecular organization at low temperatures is similar to the point-defect configuration and  $G_2(r)$  decays quickly to zero, confirming the absence of long range correlation between the particles at the center and those at a certain distance from it. Increasing the field strength the radius of the aligned core increases and correspondingly the correlations between the molecules at the center and the other particles inside the droplet remain important up to longer distances.

The change in behavior is not linear with  $\xi$ , but there is, at least at low temperature, a jump for values of  $\xi$  less than 0.03. To provide a semiquantitative indication of this effect, we have also calculated the areas under the  $G_2(r)$  curves:

$$G_2 = \int_0^{r_{\max}} G_2(r) dr. \quad (4.6)$$

The results for  $T^* = 0.4$  are reported in Fig. 7 and confirm a saturation of  $G_2$  with  $\xi$ . Going back to Fig. 6(b), we have that at high temperature ( $T^* = 1.4$ ) the system is disordered, as seen previously from other observables, and the correlation functions decay rapidly to their minimum in all cases. The residual order induced by the

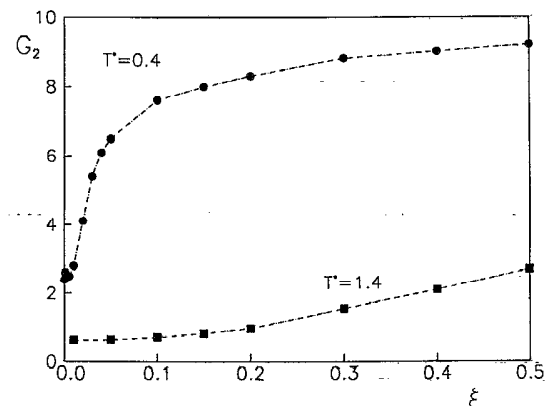


FIG. 7. The area delimited by the second-rank pair coefficient  $G_2(r)$  plotted against the field strength  $\xi$  at  $T^* = 0.4$  and 1.4.

external field is apparent [Fig. 6(b) and Fig. 7] for the higher field strengths. At low temperature the change of  $G_2$  with  $\xi$  is rather steep, with the field-induced molecular reorganization, taking place between  $\xi = 0.01$  and  $\xi = 0.1$ . Given the inevitable smoothing effect associated with simulation of a relatively small sample this is an indication of compatibility with the first order transition predicted in [15], although a steep continuous change cannot be ruled out.

### V. MOLECULAR ORGANIZATION AND DEUTERIUM NMR LINE SHAPES

As mentioned before, Monte Carlo simulations allow us to generate as output, apart from numerical results for the averages of thermodynamic observables described in Sec. IV, full sets of coordinates and angles representing instantaneous configurations of the lattice. The snapshots of some of the configurations found are shown in Fig. 8. Two sections, an equatorial (left) and a vertical (right) one, are reported and from these it is possible to observe qualitatively how the molecular organization is influenced by the application of the external field.

It is interesting to observe the similarity with the configurations obtained by Lavrentovich *et al.* [37,38] in their experimental studies of the positive dielectric anisotropy material 4-cyano-4'-*n*-pentyl-biphenyl (5CB) in electric fields. These data were, however, obtained with much larger droplets ( $r \geq 20 \mu m$ ) and in that system the ordering along the field is probably eased also by the electric conductivity anisotropy. Configuration data are also useful for calculating off line other quantities of interest. In particular from the configurations, given as a set of direction cosines, we have calculated polydomain deuterium NMR line shapes for our system of fictitious molecules.

Deuterium NMR of deuterated liquid crystals has been frequently used in studying PDLC droplets [4,6,7], particularly when the droplets are so small that standard optical methods are not viable. The use of  $^2H$  NMR allows focusing on the molecules inside the droplet (the only deuterated ones) thus giving in principle a direct handle on their properties. Each deuteron with quadrupole coupling constant  $\nu_Q$  and angle  $\theta$  between the effective quadrupole axis and molecular axis provides a couple of transitions at the frequency

$$\omega_Q(\cos \beta_i) = \pm \frac{3}{4} \nu_Q P_2(\cos \beta_i) P_2(\cos \theta), \quad (5.1)$$

where  $\beta_i$  is the angle between molecule and field axis, and uniaxial symmetry of the tensor and of the molecule is assumed. If the effect of the NMR spectrometer magnetic field on the configuration is negligible, as is the case at least for submicrometer droplets [19], then field effects due to the applied external field can be examined.

Moreover, if molecular diffusion can be assumed to be negligible at the chosen experimental conditions, then the deuterium NMR spectrum becomes a powderlike one and can give information on the director distribution or more generally on the molecular organization. These ap-

parently rather stringent conditions have been shown to hold in various experimental studies [6,7].

In order to calculate simulated line shapes from the Monte Carlo configurations we have assumed a system of fictitious deuterated molecules with axis of effective molec-

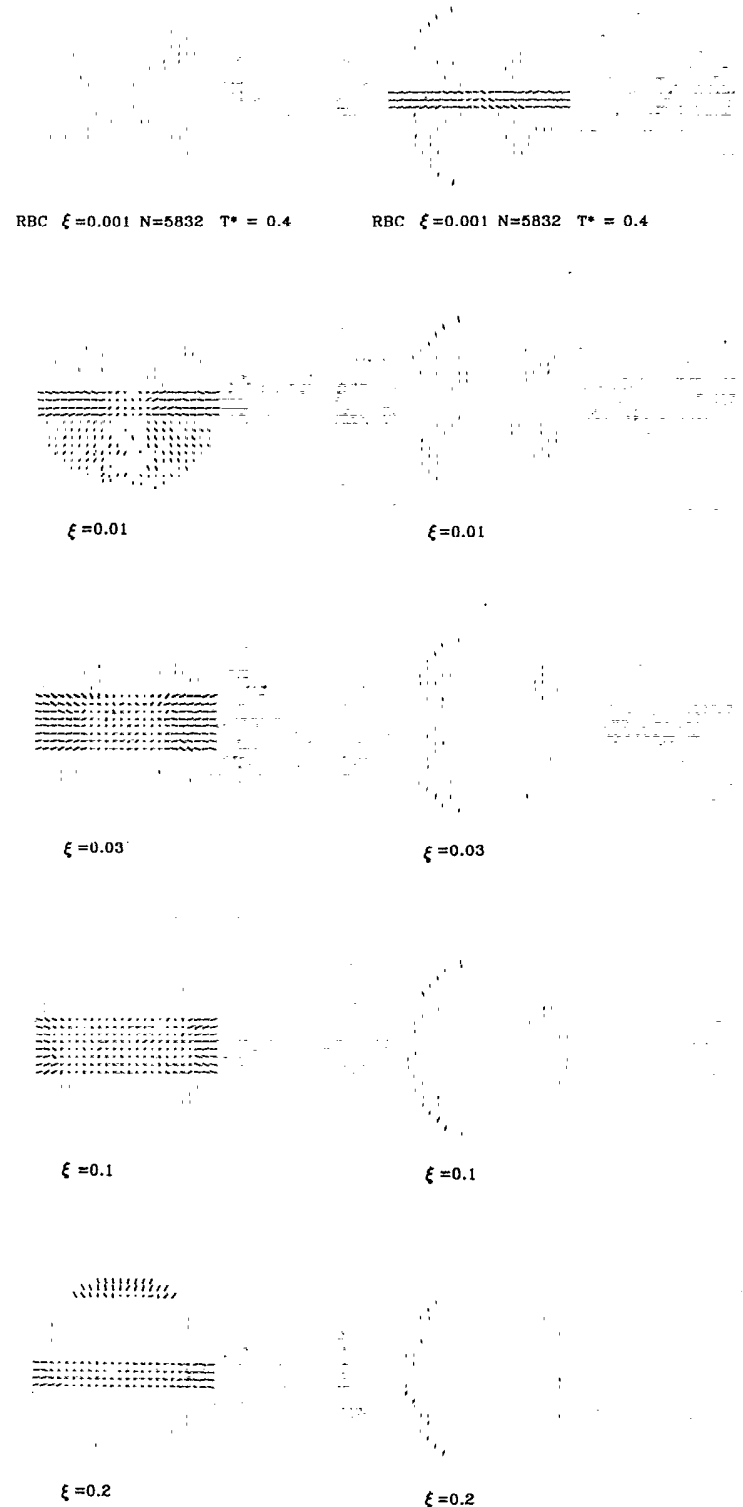


FIG. 8. Snapshots of typical droplet configurations for five different field strengths at temperature  $T^* = 0.4$ . For each case an equatorial and a vertical section are reported.

ular uniaxial symmetry corresponding to the axis of our particles as obtained for our configurations. As already mentioned, diffusion effects are neglected and every line shape is obtained as an average over a set of different configurations at the same temperature.

The total spectrum for a configuration is calculated as the sample average

$$S(\omega) = \langle S(\omega, \omega_Q(\cos \beta_i), T_2^{-1}) \rangle_S \quad (5.2a)$$

$$= \frac{1}{N} \sum_{i=1}^N S(\omega, \omega_Q(\cos \beta_i), T_2^{-1}). \quad (5.2b)$$

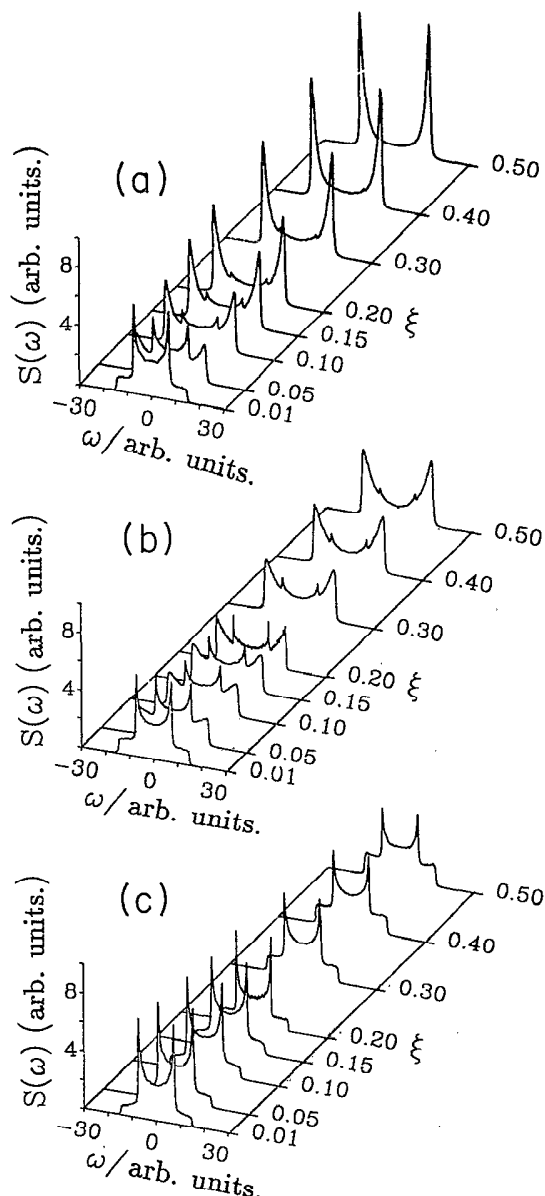


FIG. 9. Polydomain deuterium NMR line shapes calculated from the molecular organizations obtained by Monte Carlo simulation. Results for various field strengths are shown at a (a) "low" ( $T^* = 0.4$ ), (b) "intermediate" ( $T^* = 1.0$ ), and (c) "high" temperature ( $T^* = 1.7$ ). The frequency is given in arbitrary units (see text).

Every particle provides a line shape contribution

$$S(\omega, \omega_Q(\cos \beta_i), T_2^{-1}) = \frac{T_2^{-1}}{[\omega - \omega_Q(\cos \beta_i)]^2 + [T_2^{-1}]^2} + \frac{T_2^{-1}}{[\omega + \omega_Q(\cos \beta_i)]^2 + [T_2^{-1}]^2}, \quad (5.3)$$

We assume for each line a Lorentzian shape with the intrinsic linewidth  $T_2^{-1} = 200$  Hz. In our calculations we have used data appropriate to 4'-methoxy-4-cyanobiphenyl- $d_3$  (10CB):  $\nu_Q = 175$  kHz and  $\theta = 59.45^\circ$  corresponding to the angle between the  $CD_3$  axis and the molecular axis and consistently with the assumption of fast rotation of the  $CD_3$  group, as from Ref. [6]. This allows a correspondence with kHz of the arbitrary units used for the frequency scale. The resulting spectrum is then further averaged over a number of configurations to improve the signal to noise ratio.

The NMR line shapes calculated from an average over ten droplet configurations of the large ( $N = 5832$ ) droplets at different field strengths and at three temperatures are given in Fig. 9. The deuterium NMR spectrum corresponds to a superposition of doublets originating from each molecule in the droplet.

The deuterium splitting has the greatest magnitude when the molecules have their principal axis parallel to the applied field. For the low temperature case [Fig. 9(a)], at the lowest field, the droplet configurations is characterized by a nearly perfect star configuration and it gives rise to a line shape characteristics of an essentially three dimensional isotropic distribution of molecules with respect to the direction of the applied field. At stronger fields the population of molecules parallel to the field increases and the line shape essentially reduces to a doublet corresponding to the parallel splitting. For the higher temperatures [Figs. 9(b) and 9(c)] the line shapes obtained from the lowest field has still the characteristics of a powder spectrum. However, even for the intermediate temperature,  $T^* = 1.0$ , case, the population of molecules aligned with the field increases when higher fields are applied to the system, leading to a more complex pattern, while for the isotropic case at the highest temperature,  $T^* = 1.7$ , the line shape is almost unchanged upon increasing temperature.

## VI. CONCLUSIONS

PDLC systems on a submicrometer scale offer a fascinating possibility of constructing collective supermolecular organizations by suitably choosing boundary conditions, nematic material, and temperature.

The application of a suitable external field provides a direct way of varying and controlling this molecular organization. Here we have simulated the effect of a field on a material with positive susceptibility anisotropy and we have shown the outcome in a number of ways, from snapshots to NMR line shapes. Our results (cf. Figs. 7 and 9) show a steep change in molecular organization for field strengths between  $\xi = 0.01$  and  $\xi = 0.1$ .

## ACKNOWLEDGMENTS

We are grateful to CNR and MURST (Rome) for support of this work and to the Swedish Natural Science Research Council for support given to E.B. We

wish to thank G. Chidichimo, A. Golemme (Unical), O. Lavrentovich, and S. Žumer (Kent State) for stimulating discussions. A fruitful interaction with T.J. Sluckin (Southampton) was made possible by a British Council - MURST grant.

- [1] G.P. Crawford and J.W. Doane, *Condens. Matter News* **1**, 5 (1992).
- [2] J.W. Doane, N.A. Vaz, B.-G. Wu, and S. Žumer, *Appl. Phys. Lett.* **48**, 269 (1986).
- [3] J.W. Doane, *Mater. Res. Bull.* **16**, 22 (1991).
- [4] G. Chidichimo, G. Arabia, A. Golemme, and J.W. Doane, *Liq. Cryst.* **5**, 1443 (1989).
- [5] P.S. Drzaic, *J. Appl. Phys.* **60**, 2142 (1986).
- [6] A. Golemme, S. Žumer, J.W. Doane, and M.E. Neubert, *Phys. Rev. A* **37**, 559 (1988).
- [7] R. Aloe, G. Chidichimo, and A. Golemme, *Mol. Cryst. Liq. Cryst.* **203**, 1155 (1991).
- [8] N. Schopohl and T.J. Sluckin, *J. Phys. (Paris)* **49**, 1097 (1988).
- [9] H. Mori and H. Nakanishi, *J. Phys. Soc. Jpn.* **57**, 1281 (1988).
- [10] E. Penzenstadtler and H.-R. Trebin, *J. Phys. (Paris)* **50**, 1027 (1989).
- [11] C. Chiccoli, P. Pasini, F. Semeria, and C. Zannoni, *Phys. Lett. A* **150**, 311 (1990).
- [12] C. Chiccoli, P. Pasini, F. Semeria, and C. Zannoni, *Mol. Cryst. Liq. Cryst.* **212**, 197 (1992).
- [13] C. Chiccoli, P. Pasini, F. Semeria, and C. Zannoni, *Mol. Cryst. Liq. Cryst.* **221**, 19 (1992).
- [14] E. Berggren, C. Zannoni, C. Chiccoli, P. Pasini, and F. Semeria, *Chem. Phys. Lett.* **197**, 224 (1992).
- [15] E. Dubois-Violette and O. Parodi, *J. Phys. (Paris) Colloq.* **30**, C4-57 (1969).
- [16] J.H. Erdmann, S. Žumer, and J.W. Doane, *Phys. Rev. Lett.* **64**, 1907 (1990).
- [17] A.V. Koval'chuck, M.V. Kurik, O.D. Lavrentovich, and V.V. Sergan, *Zh. Eksp. Teor. Fiz.* **94**, No. 5, 350 (1988) [*Sov. Phys. JETP* **67**, 1065 (1988)].
- [18] R. Ondris-Crawford, E.P. Bokyo, B.G. Wagner, J.H. Erdmann, S. Žumer, and J.W. Doane, *J. Appl. Phys.* **69**, 6380 (1991).
- [19] G.P. Crawford, R. Ondis-Crawford, S. Žumer, and J. W. Doane, *Phys. Rev. Lett.* **70**, 1838 (1993).
- [20] F. Xu, H.-S. Kitzerow, and P.P. Crooker, *Phys. Rev. A* **46**, 6535 (1992).
- [21] P.A. Lebowitz and G. Lasher, *Phys. Rev. A* **6**, 426 (1972).
- [22] U. Fabbri and C. Zannoni, *Mol. Phys.* **58**, 763 (1986).
- [23] D.J. Cleaver and M.P. Allen, *Phys. Rev. A* **43**, 1918 (1991).
- [24] Z. Zhang, O. Mouritsen, and M.J. Zuckermann, *Phys. Rev. Lett.* **69**, 2803 (1992).
- [25] W.H. de Jeu, *Physical Properties of Liquid Crystalline Materials* (Gordon and Breach, New York, 1980).
- [26] G.R. Luckhurst, P. Simpson, and C. Zannoni, *Chem. Phys. Lett.* **78**, 429 (1981).
- [27] G.R. Luckhurst and P. Simpson, *Chem. Phys. Lett.* **95**, 149 (1983).
- [28] J. Hanus, *Phys. Rev.* **178**, 420 (1969).
- [29] S. Marčelja, *Nature* **241**, 451 (1973).
- [30] C. Zannoni, *The Molecular Physics of Liquid Crystals*, edited by G.R. Luckhurst and G.W. Gray (Academic, London, 1979), Chap. 9, p. 191.
- [31] D. E. Knuth, *The Art of Computer Programming* (Addison-Wesley, Reading, MA, 1981), Vol. 2.
- [32] J.A. Barker and R.O. Watts, *Chem. Phys. Lett.* **3**, 144 (1969).
- [33] C. Zannoni, *J. Chem. Phys.* **84**, 424 (1986).
- [34] A. Golemme, S. Žumer, D.W. Allender, and J.W. Doane, *Phys. Rev. Lett.* **61**, 2937 (1988).
- [35] S. Žumer, M. Vilfan, and I. Vilfan, *Liq. Cryst.* **3**, 947 (1988).
- [36] C.L. Jackson and G.B. McKenna *J. Chem. Phys.* **93**, 9002 (1990); *J. Non-Cryst. Solids* **131-133**, 221 (1990).
- [37] V.G. Bodnar, A.V. Koval'chuck, O.D. Lavrentovich, V.M. Pergamenschik, and V.V. Sergan, *Proc. SPIE* **1455**, 61 (1991).
- [38] V.G. Bodnar, O.D. Lavrentovich, and V.M. Pergamenschik, *Zh. Eksp. Teor. Fiz.* **101**, 111 (1992) [*Sov. Phys. JETP* **74**, 60 (1992)].